Title

Gold-Decorated M13 I–Forms and S–Forms for Targeted Photothermal Lysis of Bacteria

Journal

ACS Applied Materials & Interfaces, 12(1)

ISSN

1944-8244

Authors

Ngo-Duc, Tam-Triet

Alibay, Zaira

Plank, Joshua M

et al.

Publication Date

2020-01-08

DOI

10.1021/acsami.9b15682

Peer reviewed

Citation: *ACS Applied Materials & Interfaces 2020 12 (1), 126-134*

Gold-decorated M13 I-forms and S-forms for Targeted Photothermal Lysis of Bacteria

Tam-Triet Ngo-Duc[†‡], Zaira Alibay[†‡], Joshua M. Plank[§], Joseph Earl Cheeney[†], Elaine D. Haberer[†, §]

[†]Materials Science and Engineering Program, University of California, Riverside 92521, USA

[§]Department of Electrical and Computer Engineering, University of California, Riverside 92521, USA

‡These authors contributed equally.

ABSTRACT: With the emergence of multidrug resistant bacteria, photothermal therapy has been proposed as an alternative to antibiotics for targeting and killing pathogens. In this study, two M13 bacteriophage polymorphs were studied as nanoscaffolds for plasmonic bactericidal agents. Receptor-binding proteins found on the pIII minor coat protein targeted *E. coli* bacteria with F-pili (F^+ strain), while a gold-binding peptide motif displayed on the pVIII major coat protein templated Au nanoparticles. Temperature-dependent exposure to a chloroform-water interface transformed the native filamentous phage into either rod-like or spheroid structures. The morphology, geometry, and size of the polymorphs, as well as the receptor-binding protein and host cell receptor interaction were studied using electron microscopy. Au/template structures were formed through incubation with Au colloid, and optical absorbance was measured. Despite the closely packed Au nanoparticle layer on the surface the viral scaffolds, electron microscopy confirmed that host receptor affinity was retained. Photothermal bactericidal studies were performed using 532 nm laser irradiation with a variety of powers and exposure times. Bacterial viability was assessed using colony count. With the shape-modified M13 scaffolds, up to 64% of *E. coli* were killed within 20 min. These studies demonstrate the promise of i-form and s-form polymorphs for the directed plasmonic-based photothermal killing of bacteria.

1. INTRODUCTION

With the advance of multidrug resistant (MDR) bacteria, antibiotics are losing their potency. *Staphylococcus aureus (S. aureus), Escherichia coli (E. coli),* and *Pseudomonas aeruginosa (P. aeruginosa)* are a few examples of known pathogens that have developed antibiotic resistance through genetic mutations.[1–3] The development of novel long-term approaches to combat pathogenic microbial cells is necessary. Photoinduced inactivation of bacterial infections is a

promising pathway, as the method is immune to development of antibiotic resistance.[4] In this approach, light-absorbing nanoparticles are delivered to the target, and irradiated. Through localized surface plasmon resonance (LSPR), photons absorbed by these particles generate heat, which is then transferred to nearby pathogenic microbial cells, permanently damaging the cell membrane and causing cell death. In particular, gold nanostructures ranging from particles to rods to clusters have been successfully utilized as photoabsorbing agents.[5–7] These particles are non-toxic, chemically inert, and tunable over a wide range of absorption wavelengths from visible to infrared.[8,9] Illuminated by a coherent light source with power in the tens of milliwatts range, these noble metal absorbers have demonstrated rapid (≤ 30 min) photothermal killing of various MDR bacteria, thus establishing the potential of this methodology as a highly potent therapy.[10–12]

To impart specificity and aid in targeting, gold nanostructures are frequently functionalized with antibodies.[5,10,13–15] Highly selective binding between antibody and antigen facilitates concentration of photoabsorbing agents on the MDR bacteria surface, increasing photothermal bactericidal effects and minimizing injury to surrounding tissue.[16] Such precision recognition is critical for effective and efficient bacteria elimination. Despite widespread use, there are considerable challenges associated with antibody conjugation. Production of antibodies requires the use of animal models, making the process undesirably expensive and time-consuming.[17] Furthermore, antibodies are notoriously unstable, exhibiting sensitivity to temperature, pH, and ionic strength.[18] In order to ensure active structures with an orientation compatible with antigen binding, specific handling conditions must be maintained and harmful chemical conjugation strategies avoided.

Because of the drawbacks associated with conjugated antibodies, a number of alternative strategies for imparting biological specificity have been explored.[19–21] Among these is the use of viral receptor-binding proteins. These biomolecular structures interact with bacterial host cell receptors with an affinity and specificity comparable to that of antibodies with antigens.[22,23] Yet, unlike antibodies, phage-based receptor-binding proteins are readily adaptable for low-cost, large-scale manufacturing via bacterial host infection and robust under a wide range of environmental conditions.[19,24,25] Bacteriophage with well-characterized life cycles and proteomes are of specific interest as photothermal bactericidal agents. Among these is the M13, a filamentous bacteriophage. The capsid of this combinatorial phage display workhorse is comprised of five structural proteins (pIII, pV, pVII, pIX, and pVIII), each of which can be modified to display a variety of functional motifs. Notably, the pIII minor coat proteins, located at the proximal end of the virus, and the pVIII major coat proteins, found along the length of the virus body, are most commonly used for display.[26] Native receptor-binding proteins on the pIII can be used in conjunction with one or more of the other structural proteins to simultaneously target *E. coli* with F-pili (F^+ strain) and template nanoscale cargo.[27,28] During infection, receptor-binding proteins complex with bacteria cell receptors on F-pili. These hair-like appendages then retract, transporting the bacteriophage to the bacterial membrane. Because the pIII is modular with well-understood structure and function, phage host range can be readily expanded.[28–30] Chimera, incorporating binding-receptor proteins from other filamentous phage, have successfully targeted not only N^+ and I^+ strains of *E. coli*, but also *Vibrio cholerae, P. aeruginosa, and Xanthomonas campestris*.[28,30] This targeting versatility, spanning both human and plant pathogens, highlights the potential of the M13 bacteriophage to be used as a photothermal bactericidal agent for not only *E. coli*, but also a much broader range of bacteria.

While the length (~ 1 μm) of the M13 filamentous bacteriophage does not provide the desired spatial intimacy between photoabsorbing agents and target pathogens for plasmonic photothermal bactericidal agents[31], intermediate (i-form) and spheroidal (s-form) polymorphs are more promising. When exposed to a chloroform-water interface, the filamentous form of the M13 contracts, mimicking the structural changes associated with host cell infection. At low temperature (≤ 4°C), intermediate rod-like structures a few hundred nanometers in length are formed.[32,33] At room temperature, spheroids tens of nanometers in diameter are created. These unique polymorphs have been primarily studied within the context of host infection, and have been largely neglected as nanotemplates. Yet, the described geometric transformation shortens the distance between viral binding-receptor proteins and templated photoabsorbing agents, making these polymorphs potentially viable scaffolds for plasmon-induced inactivation of bacteria.

This work investigates the directed killing of bacteria using geometrically modified M13 bacteriophage as nanoscaffolds for plasmonic photothermal agents. Here, the viral capsid served two simultaneous functions. Native receptor-binding proteins found on the pIII minor coat protein targeted F^+ *E. coli* bacteria, while a gold-binding peptide motif displayed on the pVIII major coat protein templated plasmonic Au nanoparticles (NPs). A simple temperature-dependent chloroform treatment was used to convert gold-binding M13 filaments into i-form and s-form polymorphs. Electron microscopy was used to assess template morphology, geometry, and size, in addition to nanoscaffold receptor-binding protein and host cell receptor interaction. Nanoparticles were assembled in a dense layer on the template surface forming Au/template nanostructures. Electron microscopy revealed that these nanostructures retained affinity for bacterial host receptors; however Au/s-forms complexed with *E. coli* at a higher frequency and

more intimately than Au/i-forms. The photothermal bactericidal effects of the Au/templates were evaluated under 532 nm laser illumination for a range of times and power densities. While both nanostructures displayed bactericidal properties, more bacteria cell death was observed for Au/s-forms under the same illumination conditions. These studies are an initial illustration of the combined targeting specificity and photothermal bactericidal properties of gold-decorated M13 i-forms and spheroids. Given the genetic programmability of the pIII to expand targeting of receptor-binding proteins to a variety of MDR pathogens and of the pVIII to incorporate affinity peptides for a range of photoabsorbing agents, these dual-purpose nanoscaffolds have tremendous potential as a effective therapy for MDR bacterial infections.

2. EXPERIMENTAL DETAILS

2.1. M13 transformation and *E. coli* interaction. An M13 bacteriophage with a gold-binding peptide, VSGSSPDS,[34] displayed on each of approximately 2700 copies of the pVIII major coat protein found along the viral length was selected and studied as a scaffold for photothermal antibacterial agents. The gold-binding phage was transformed from its filamentous form to its spheroidal polymorph as previously described.[35] Briefly, the phage was dispersed in 100 μL tris-buffered saline (TBS, 50 mM Tris-HCl, 150 mM NaCl, pH 7.5) at a concentration of 10^8 pfu/μL and vortexed with an equal volume of chloroform (99.8%, ACROS Organics) for 5 vortex/rest (2 s/13 s) cycles at room temperature. Post transformation, 95 μL of the chloroform was removed and air was gently blown over the sample for 15 s to ensure removal of residual chloroform. M13 filaments were transformed to i-forms using a similar approach at reduced temperature.[36, 37] Prior to mixing, phage and chloroform solutions were allowed to cool to 0°C over a period of 2 min.

The phage/chloroform suspension was then vortexed at 0℃ for 5 vortex/rest (8 s/ 5 s) cycles at low power and chloroform was removed.

The *E. coli* K12 was used as a model system to assess interactions with transformed M13 phage. Both F^+ (K12 ER2738) and F^- (K12 HB101) strains were used as hosts in these studies. Bacteria cultures were grown on a shaking incubator at 350 rpm in lysogeny broth (LB broth, Lennox, Fisher BioReagents) at 37℃ for 5 to 6 h or to mid-log phase. Tetracycline hydrochloride (20 mg/mL, Genlantis) was added to the K12 ER2738 culture during growth. The optical density was measured at 600 nm and the *E. coli* cell concentration was diluted to 2 x 10^4 cells/μL. To allow attachment, a 25 μL volume of i-form or s-form polymorphs was incubated with 2.5 μL of the bacteria at 4°C for 90 min.

2.2. Gold binding on the M13 phage. To assemble Au/i-form and Au/s-form bactericidal nanostructures, transformed viral templates were decorated with Au NPs. Equal volumes of Au colloid (5 nm, 5 x 10^{10} particles/μL, BBI Solutions) and viral templates (10^8 pfu/μL) were gently vortexed, incubated for 10 min at 4°C, and used immediately.

2.3. Binding and bactericidal activity of viral-templated gold nanostructures. The effectiveness of Au/i-form and Au/s-form nanostructures in binding to bacteria was evaluated using *E. coli* K12 ER2738, an F^+ strain, at a concentration of 2 x 10^4 cells/μL. A 2.5 μL volume of F^+ *E.coli* was added to 25 μL of viral-templated gold nanostructures (Au/i-form or Au/s-form) for a final nanostructure concentration of 4.5 x 10^7 templates/μL or a 2250-fold excess of Au/template. The solutions were incubated for 90 min at 4°C in the dark to allow bactericidal agents to bind, and samples were prepared for TEM analysis. To assess the role of the F-pilus in Au/i-form and Au/s-form attachment, similar experiments were performed with *E. coli* K12 HB101, an F^- strain.

To evaluate Au/templates as photothermal antibacterial agents, the same binding procedure was used to make duplicate solutions of each viral-templated gold nanostructure with F^+ *E. coli*. Subsequently, one of each of the duplicate mixtures was transferred to an open polymerase chain reaction (PCR) tube and exposed to continuous wave 532 nm laser illumination (Horiba LabRam/AIST-NT AFM) with a spot size of 0.2 cm^2. Both illuminated and unilluminated solutions were diluted to ~ 4 x 10^2 cells in LB broth, plated on agar, and incubated at 37°C for 14 h. Bacteria colonies were counted, and *E. coli* viability (%) for both Au/i-forms and Au/s-forms was calculated by normalizing the number of colonies on the illuminated plate to the number of colonies on the unilluminated plate. The effect of a range of laser power densities (0, 100, 200, and 300 mW cm^{-2}) and illumination times (0, 5, 12, and 20 min) on cell viability was explored. To ensure that the viral-templated gold nanostructures and their nanoscale building blocks were not fundamentally detrimental to bacteria (irrespective of 532 nm laser exposure), viability was also determined for unilluminated control solutions of *E. coli* K12 ER2738 incubated with Au/i-forms, Au/s-forms, i-forms, s-forms, and gold colloid. Experiments were repeated in triplicate.

The bulk solution temperature was measured at the maximum laser illumination dose for both Au/i-forms and Au/s-forms using an infrared camera (OPTRIS PI160) with a spot size resolution of 1.5 mm. The solution temperature measurements were performed before and after exposure to 300 mW/cm^2 continuous wave 532 nm laser illumination for 20 min.

2.4. Transmission electron microscopy. Transmission electron microscopy (TEM, Tecnai T12) was used to characterize the shape and dimensions of transformed viral templates, evaluate the ability of i-form and s-form polymorphs to bind *E. coli* F-pili before and after incubation with Au NPs, and count Au/i-forms and Au/s-forms on the bacteria surface. In addition, electron microscopy was used to determine the role of the F-pilus in attachment of Au/templates to *E.*

coli. For these studies, 5 μL of sample was pipetted onto a formvar/carbon-coated copper grid (Ted Pella, Inc.) and incubated for 5 min. The grids were then rinsed twice with deionized water, stained with 2% uranyl acetate for 30 s, and wicked dry with filter paper. TEM images of the samples were analyzed using ImageJ software. A segmented line function was used to measure the length and width of the templates. Structures with an aspect ratio between 3 and 25 with lengths between 80 and 300 nm were defined as i-forms, whilst geometries with aspect ratios < 3 were denoted as spheroids.[35]

2.5. Ultraviolet-visible (UV-vis) spectroscopy. Optical absorbance spectroscopy (Evolution 60, ThermoFisher) was used to measure M13 bacteriophage and bacteria concentrations, the absorbance spectra of the Au/i-forms and Au/s-forms, and to estimate the number of gold nanoparticles per template. OD_{269} and OD_{600} were used to measure the concentrations of filamentous phage and bacteria, respectively, according to previously published procedures.[26] The absorbance of viral-templated gold nanostructures and 5 nm Au colloid was measured from 200 to 1000 nm using a quartz cuvette with a 10 mm optical pathlength. Prior to UV-vis measurements, the Au colloid was diluted in TBS to achieve a final Au NP concentration similar to that used in viral-templated gold nanostructure assembly. Finally, to approximate the global number of Au NPs per template, solutions of assembled Au/i-form and Au/s-form bactericidal nanostructures were centrifuged at 50 rcf for 30 min, leaving unbound Au NPs suspended within the supernatant. The absorbance of the unbound particle solution was measured, as well as the absorbance of the Au colloid without viral templates. The difference between the two absorbance measurement peaks was used to calculate the number of NPs per template. Measurements were taken on three independent samples and averaged.

3. RESULTS AND DISCUSSION

A schematic overview of Au/i-form and Au/s-form bactericidal nanostructure assembly, F^+ *E. coli* targeting, and subsequent killing of bacteria via photothermal lysis is shown in Figure 1. Brief chloroform exposure was used to convert the native filamentous form of the M13 gold-binding bacteriophage to i-form and s-form polymorphs. The transformation temperature dictated the template geometry, with low temperature (0°C) and room temperature processes yielding rods and spheroids, respectively. Due to the thousands of gold-binding peptide fusions displayed on pVIII major coat proteins, viral-templated gold nanostructures were created through the simple addition of 5 nm Au NPs to the transformed phage solution. These inactive, gold-decorated, morphologically transformed phage successfully targeted F^+ *E. coli* through F-pili binding. Retraction of F-pili assisted delivery of bactericidal nanostructures to the cell surface. Once these gold clusters were adjacent to the cell membrane, 532 nm laser illumination was used to photothermally kill the bacteria.

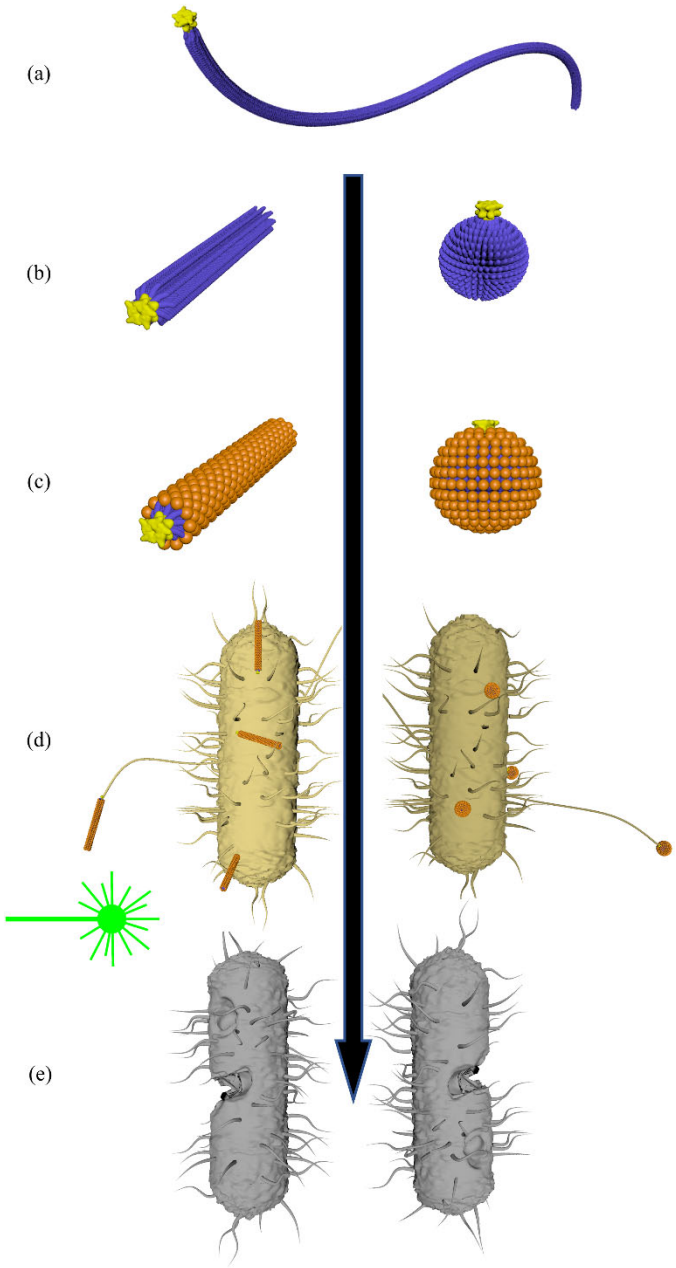

Figure 1. Schematic illustration of the (a) gold-binding M13 filamentous phage, (b) transformed phage templates (i-form and s-form), (c) Au NPs decorating the Au/i-form and Au/s-form, (d) targeted binding and delivery of photothermal antibacterial agents to cell surface via *E. coli* F-pili, and (e) destruction of bacteria by laser illumination. The five copies of the pIII minor coat proteins located on the proximal tip of the virus, on which the receptor-binding proteins are

found are shown in yellow. The approximately 2700 copies of the pVIII major coat protein that comprise the capsid body are shown in blue.

Geometrically-transformed, gold-binding M13 bacteriophage were studied with TEM as templates for bactericidal nanostructures. The distinctive morphologies of the M13 i-form and s-form polymorphs are shown in Figure 2 and Figure 3, respectively. As a point of comparison, a few images of gold-binding filaments have been included in the Supporting Information (Figure S1). The average length of this viral mutant is 912 ± 14 nm.[35] As revealed in Figure 2, gold-binding M13 i-forms displayed a tube-like structure with one closed, rounded tip of slightly varying curvature and one open, flat or flared end. The morphology is consistent with other low temperature M13 transformation studies.[36,37] In these reports, the flared end was identified as the location through which DNA is extruded during infection and site of the pIII minor coat protein.[36,38,39] The average length of the gold-binding i-forms was 161 ± 33 nm (Figure S2). This represents a 5.7-fold decrease in length compared to the filamentous form. It is interesting to note that the average gold-binding i-form length is significantly less than the 250 nm length measured for the wild-type i-form.[33] This difference may be a simple function of transformation conditions. Alternatively, it could be associated with differences in pVIII-pVIII interactions within gold-binding and wild-type phage attributable to the peptide fusion. Additional investigation is necessary to discern the source of disparity. As illustrated in Figure 3, using electron microscopy, gold-binding s-forms appeared as round, but slightly deflated or distorted spheroids with an average size of approximately 60 nm. Deviations from spherical geometry were attributed to drying effects associated with sample preparation, and have been reported by a number of other authors[39–41]. In some cases, a small opening could be seen in the wall of the

spheroids. Other studies have linked this hole to the release of viral DNA, and consequently to the pIII position.[36,38] Spheroid size and morphology were consistent with our previous studies which described the room temperature transformation of gold-binding phage in detail.[35]

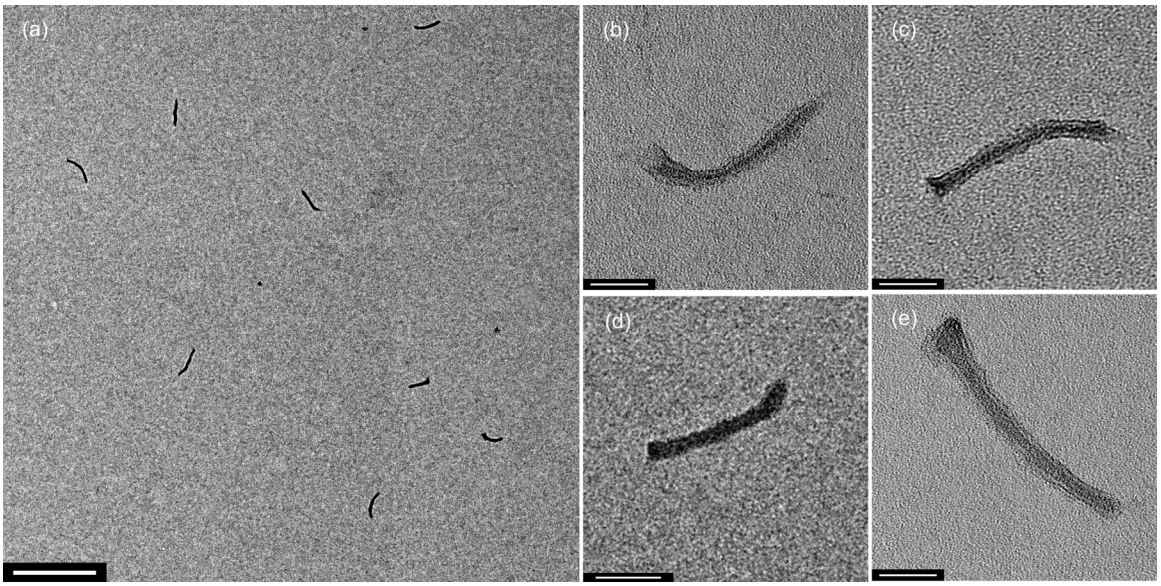

Figure 2. Electron micrographs of gold-binding M13 bacteriophage i-forms exhibiting (a) a range of observed morphologies and (b-e) the characteristic hollow, rod structure with one closed, rounded tip and one open, flared end. Samples were stained with 2% uranyl acetate. (a) Scale bar: 500 nm; (b-e) Scale bar: 100 nm.

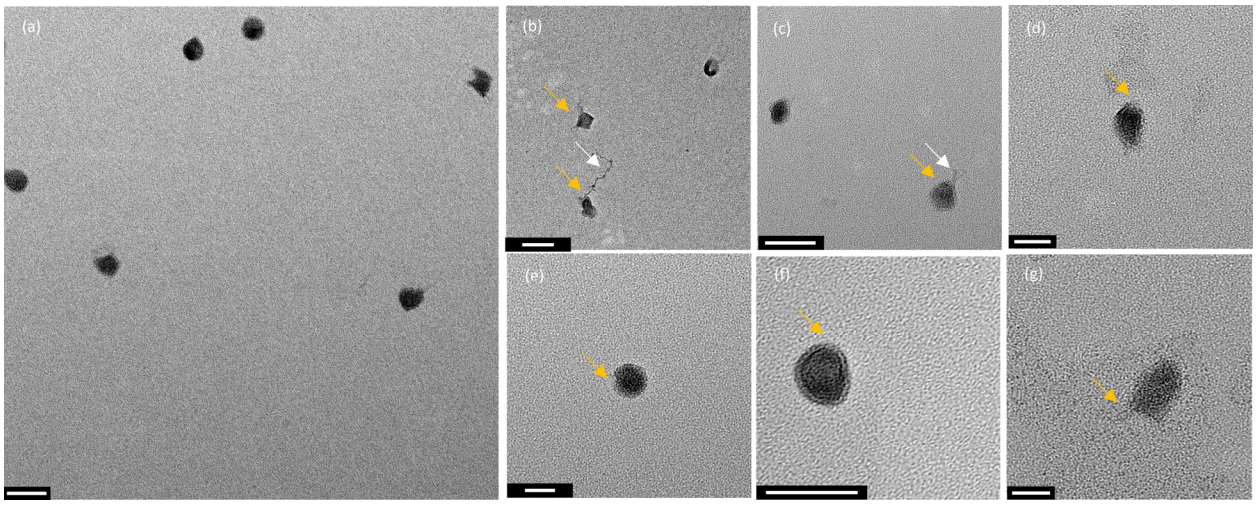

Figure 3. Electron micrographs of gold-binding M13 bacteriophage s-forms showing (a) a range of observed morphologies, in addition to the hole in the viral wall (b-c) with and (d-g) without extruded DNA present. Yellow and white arrows designate the viral wall opening and the released DNA, respectively. Samples were stained with 2% uranyl acetate. Scale bar: (a-c) 100 nm; (d-g) Scale bar: 50 nm.

In order for the genetically modified i-forms and s-forms to successfully target bacterial cells, the receptor-binding protein on the pIII must be both exposed to the environment and maintain affinity for the intended pathogen. The i-form of the wild-type f1 bacteriophage, another Ff filamentous virus, has shown evidence of anti-pIII antibody decoration.[37] Yet, there have been no direct reports of i-form or s-form pIII complexation with F-pili. To assess template-host interactions, chloroform-treated phage templates were incubated with F^+ *E. coli* at 4°C to facilitate attachment of phage to bacteria. Figures 3a and 3b show the transformed viral templates bound to the tip of a hair-like appendage protruding from the surface of the bacterial membrane. In Figure 4a, the adsorption occurred at the flared end of the i-form; while in Figure 4b, the adsorption occurred adjacent to an opening in the s-form capsid. The adsorption of the

viral templates at both locations supports pIII complexation, as prior reports confirm that this minor coat protein is found at these morphological locations[38,40]. Furthermore, it indicates that the function of the receptor-binding protein is unaffected by the transformation procedure, as it is this portion of the minor coat protein that enables host cell receptor complexation.[42]

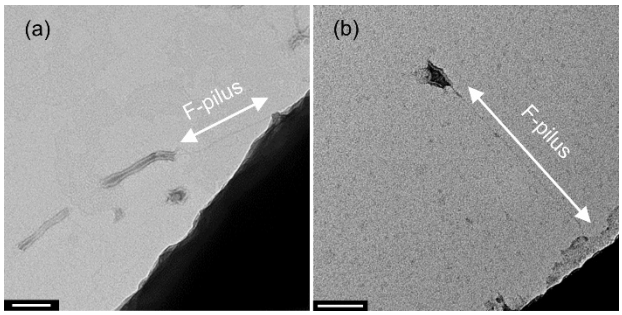

Figure 4. Gold-binding M13 bacteriophage (a) i-form and (b) s-form adsorbed to tip of *E. coli* F-pili. The associated *E. coli* K12 ER2738 cell is shown in the bottom right corner of each image. Samples were stained with 2% uranyl acetate. Scale bar: 100 nm.

Transformed gold-binding M13 bacteriophage were decorated with Au NPs to serve as photothermal antibacterial agents. Viral-templated gold nanostructures are shown in Figure 5. More examples of the nanostructures are shown in Figure S3 and S4. Colloidal Au NPs were bound to i-forms and s-forms in a disorganized, but tightly-packed arrangement which replicated the morphology of the underlying scaffold. Using UV-vis absorbance spectroscopy, an estimated 111 ± 17 NPs per s-form and 99 ± 21 Au NPs per i-form were found, yielding a fusion peptide:nanoparticle ratio significantly larger than 1:1. The optical absorbance of Au colloid, Au/i-forms, and Au/s-forms are shown in Figure 6. The LSPR or peak visible absorbance of the unbound 5 nm Au NPs was 520 nm. In comparison, the resonance peaks of the Au/i-forms and Au/s-forms were redshifted 28 and 30 nm, respectively. In addition, notable peak broadening was observed. Measured optical absorbance was a consequence of coupled plasmon modes from

the tightly-packed Au NPs on the scaffolds and the resonance of unbound Au NPs.[43–46] The broad absorbance associated with the Au/i-forms and Au/s-forms peaked near 548 nm and 550 nm, respectively, such that these structures were well-suited for 532 nm laser activation of photothermal bactericidal properties. This activation wavelength is outside of the high transparency, near-infrared windows of human tissue (650 – 850 nm and 950 – 1350 nm) and, therefore, is not compatible with applications that require deep light penetration.[47] Nonetheless, it may be useful for non-treatment based or near-surface tissue treatment applications such as the detection of food pathogens[48] or in the dispersion of bacterial biofilms[49] . Furthermore, because gold-binding peptide affinity is independent of nanoparticle shape and size, the activation wavelength for this approach can be tuned through particle selection. As demonstrated in Figure S5, both the gold-binding i-form and s-form polymorphs were also able to template large anisotropic particles with a longitudinal absorption peak at 800 nm, allowing for the future expansion of photoactivation wavelength range.

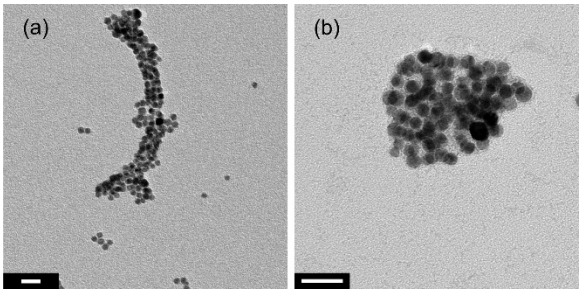

Figure 5. Gold-binding M13 bacteriophage (a) i-form and (b) s-form decorated with 5 nm Au NPs. Several unbound NPs were also observed. Scale bar: 20 nm.

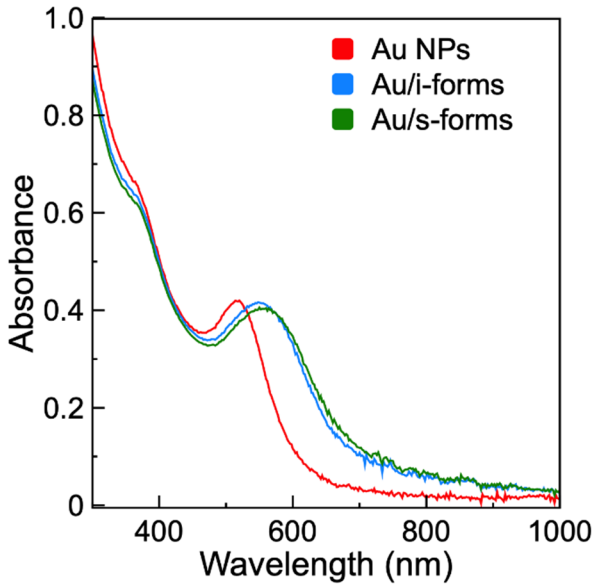

Figure 6. UV-Vis absorbance spectra of 5 nm Au NP colloidal solution, as well as Au NPs assembled on gold-binding i-form and s-form M13 bacteriophage.

The high density of gold colloid on the capsid surface necessitated additional investigation to confirm that complexation via receptor-binding protein adsorption was still achievable. Viral-templated gold bactericidal nanostructures were gently mixed with a culture of F^+ *E. coli* at 4°C. As shown in Figure 7, Au/i-forms and Au/s-forms were found both complexed with the tip of the extended F-pili and adjacent to the cell surface. Au/i-forms were attached to the cell membrane of approximately 50% of *E. coli* (N = 40). Au/i-forms experienced considerable agglomeration, frequently binding to F-pili as aggregates of several i-forms rather than as individual nanostructures. Nonetheless, the rather loose aggregates of Au/i-forms, several hundred nanometers in size, appeared to be transported to the cell surface by F-pili retraction. As shown in Figure S6, the overall proximity of the Au/i-forms to the *E. coli* was highly variable. Some agglomerates were in intimate contact with the cell surface, while others were in an extended

conformation with only a small point of contact and the bulk of the Au/i-form aggregate structure far from the surface.

In contrast, Au/s-forms were not as prone to agglomeration (Figures 7b, 7d and S7). About 79% of *E. coli* displayed surface-bound Au/s-forms (N = 38); 61% presented individual or small ensembles of up to three spheroids, while large agglomerates were seen on the remaining 18%. Drawn to the *E. coli* surface by F-pili, individual and ensembles of Au/s-forms were typically in close contact with the cell, whereas agglomerates were in a less compact, more expanded configuration. The percentage of surface-bound Au/s-forms is consistent with reports of f1 bacteriophage, a Ff class bacteriophage closely related to the M13, incubated with F^+ *E. coli* at 0°C[50]. In those studies, 77% of *E. coli* had f1 attached to at least one pilus.

It is interesting to note that, at reduced temperatures (< 25°C), the dynamic elongation and retraction of F-pili is slowed or inhibited[51,52]. Instantaneous observations, such as those produced by electron microscopy, show a fraction of *E. coli* without F-pili [50,52–54]. For example, an in depth study of F-pili activity described a range of 0 to 12 per cell when *E. coli* K12 was incubated at 0°C[50]. Likewise, in a separate investigation, an average of 0.7 F-pili per cell was reported for chilled *E. coli* K12[52]. While this condition is transient at physiological temperature, low binding temperatures prolong the existence of these pili-free F^+ bacteria likely artificially suppressing Au/template binding rates compared to higher temperatures.

Despite the high density of Au NPs on the template surface and the formation of aggregates, phage-bacteria complexes still formed between the receptor-binding protein and host cell receptor, allowing for the post-transformation targeting of F^+ *E. coli*. As a control, untemplated colloidal Au NPs were also incubated with F^+ *E. coli*. No large groups of Au NPs were observed either in solution or bound to the bacteria (Figure S8).

The template-host interaction mechanism was studied further using *E. coli* K12 HB101, a strain lacking F-pili. Following incubation, significantly fewer bacteria were found with complexed Au/templates; only 4% and 6% of F^- *E. coli* had Au/i-forms (N = 28) and Au/s-forms (N = 31) adjacent to the cell membrane, respectively. The diminished interaction between viral-templated bactericidal agents and a host lacking F-pili corroborates our findings for chloroform-treated phage templates prior to Au NP decoration. Au/template binding is largely dependent on F-pili complexation.

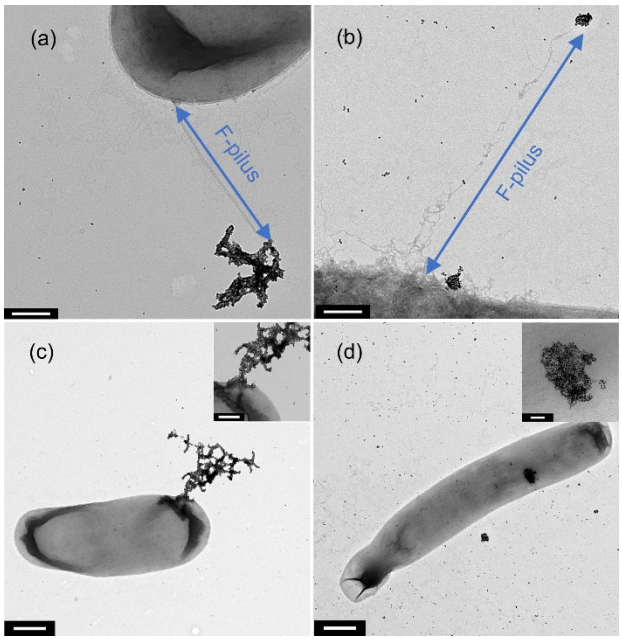

Figure 7. Au/templates bound to F-pili via pIII binding for (a) i-forms and (b) s-forms. Scale bar: 200 nm. (c) Au/i-forms and (d) Au/s-forms attached to the surface of *E. coli* demonstrating retraction of F-pili with Au/templates. Scale bar: 500 nm. Insets: Magnified images of (c) Au/i-forms and (d) Au/s-forms near cell surface. Scale bar: 100 nm. Samples were stained with 2% uranyl acetate.

The effectiveness of Au/i-forms and Au/s-forms as photothermal antibacterial agents was assessed using 532 nm laser illumination. The two viral-templated gold nanostructures were incubated with F^+ *E. coli* in the dark at 4°C for 90 min, then irradiated with coherent light for a range of times and laser powers. As shown in Figure 8, dose-dependent cell viability was used to quantify photothermal cell killing. Bactericidal effects were observed for both Au/templates. Au/i-forms produced a slow, nearly linear decline in viability with both time and power density. In contrast, Au/s-forms generated a trend with two distinct slopes. The bactericidal effects of Au/s-forms slowed considerably after 10 min of laser illumination or with greater than 200 mW/cm^2 power density. Using the maximum dose studied (20 min, 300 mW/cm^2), only 79 ± 4% and 36 ± 5% of *E. coli* survived treatment with Au/i-forms and Au/s-forms, respectively. Notably, little to no cell death was recorded for the control sample, which utilized gold colloid alone; therefore, the presence of a viral template was critical to gold nanostructure bactericidal performance. Moreover, strong bactericidal effects were only detected with laser illumination (Figure S9).

The killing mechanism associated with the Au/templates was likely thermal damage or disruption of the cell membrane caused by nanoparticle plasmonic heating.[55] While bulk solution temperatures for Au/i-forms ($T_{initial}$ = 17.91 ± 0.06°C; T_{final} = 18.75 ± 0.05°C), Au/s-forms ($T_{initial}$ = 19.32 ± 0.05°C; T_{final} = 19.5 ± 0.17°C), and Au NPs ($T_{initial}$ = 19.60 ± 0.04°C; T_{final} = 17.98 ± 0.16°C) did not measurably increase under 20 min, 300 mW/cm^2 illumination conditions, the local temperature rise generated by thermalized LSPR electrons can be substantial. LSPR-associated temperature increases are inversely proportional to the distance from the center of the particle, achieving a maximum at the particle surface and declining rapidly within 10s to 100s of nanometers.[56,57] For this reason, photothermal antibacterial agents that are not in close proximity

to the target, such as the gold colloid used in the control sample, are not generally very effective. Likewise, the comparatively low antibacterial activity of Au/i-forms can be ascribed to the relatively large spatial separation of these nanostructures from the cell surface. Specifically, the limited contact area of the Au/i-forms with bacteria, in conjunction with the reduced complexation caused by template agglomeration likely diminished overall photothermal effects. Moreover, the slowed bactericidal effects of Au/s-forms from 10-20 min and 200-300 mW/cm^2 were attributed to the small percentage of *E. coli* with attached, but more remote agglomerate configurations. The dose-dependence of Au/template bactericidal effects suggests that protracted illumination time or increased power density can be used to capitalize on long-range heating caused by distant agglomerates. In addition, photothermal cell killing may benefit from higher binding incubation temperatures (37°C). Unlike lower temperatures, physiological temperature supports constant, cyclic elongation and retraction of F-pili, potentially increasing binding percentage over time by increasing attachment and reducing the time-integrated number of pili-free F^+ bacteria[50–52,58].

In addition to the spatial intimacy with the target enabled by the receptor-binding protein on the pIII, the assembly of Au NPs on the viral template may have also boosted bactericidal performance. Heating associated with an individual nanoparticle can be amplified, under specific conditions, by modifying particle separation distance. An increase in local particle density, electromagnetic coupling of nearby particles, and growth in effective particle size due to cluster formation, all of which are potential byproducts of i-form and s-form polymorph viral assembly, can trigger higher maximum temperatures[59,60] and more effectively kill bacteria.

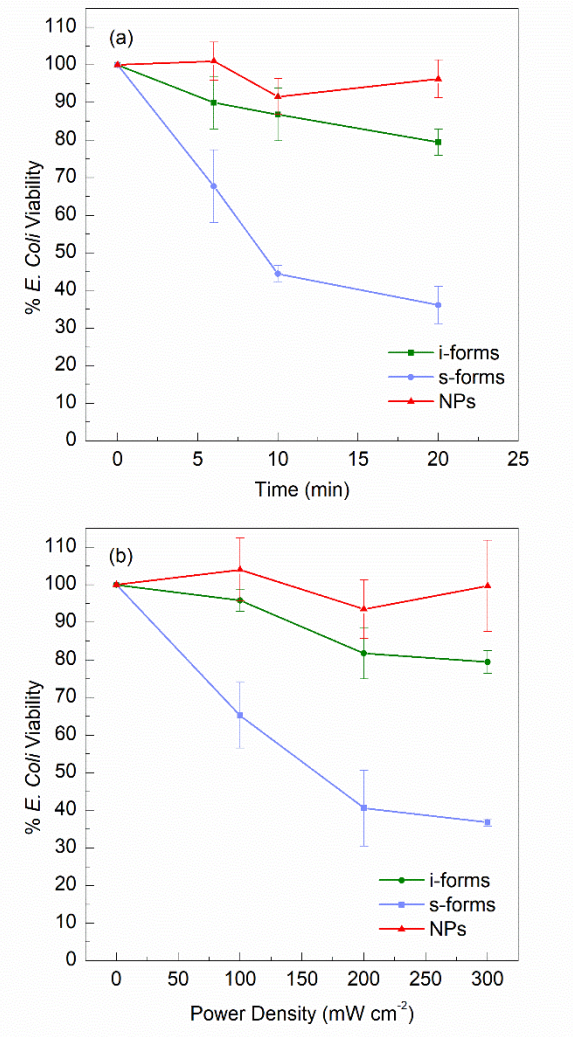

Figure 8. Photothermal bactericidal effect of Au/i-forms, Au/s-forms, and Au NPs as a function of (a) exposure time at 300 mW cm^{-2} and (b) power density using an exposure time of 20 min. Error bars represent the standard deviation over a triplicate data set.

Using laser fluence as a point of comparison, the plasmonic photothermal antibacterial activity of gold-decorated M13 i-forms and s-forms was on par with antibody-conjugated Au NPs illuminated with coherent visible or near infrared light. Here, the greatest bactericidal effects (Au/s-forms, 64% cell death) were achieved with 20 min of continuous wave 532 nm

illumination at 300 mW cm^{-2}, or a fluence of 360 J cm^{-2}. Using popcorn-shaped Au NPs functionalized with monoclonal antibodies and 1 W cm^{-2} laser irradiation at 670 nm, Lin et al. attained about 48 and 100% killing of *Salmonella DT104* for irradiation times of approximately 5 and 30 min, respectively. This is a fluence equivalence of 300 and 1800 J cm^{-2}. Millenbaugh et al. used antibody-conjugated Au NPs to photothermally kill *S. aureus.* After exposing the bacteria suspension to a 532 nm pulsed laser (100 pulses with 5 J cm^{-2} per pulse or 500 J cm^{-2} fluence), a killing efficiency of 69% and 42% for methicillin-sensitive *S. aureus* and methicillin-resistant *S. aureus*, respectively, was measured.[10] Zharov et al. also demonstrated the bactericidal effects of antibody-conjugated Au NPs on *S.aureus* using 532 nm pulsed laser light. Over 90% of bacteria was killed after exposure to 100 pulses with 3 J cm^{-2} per pulse or a total fluence of 300 J cm^{-2}.[5]

4. CONCLUSION

In conclusion, we have examined M13 gold-decorated bacteriophage polymorphs as photothermal bactericidal agents for F^+ *E. coli* bacteria. The complexation of gold-binding i-forms and s-forms was explored with and without a dense layer of surface-bound Au NPs. In both cases, despite dramatic morphological changes from filament to rod-like or spheroidal structures, receptor-binding proteins associated with the pIII minor coat proteins readily complexed with host cell receptors. This finding was significant, as it not only facilitated pathogen targeting for the photothermal bactericidal studies in this work, but also established the potential utility of polymorph receptor-binding proteins as antibody alternatives. Interestingly, due to template geometry and nanostructure agglomeration, we observed that Au/i-forms were often in less intimate contact with the host cell surface. The photothermal bactericidal activity of

the Au/template nanostructures was evaluated under 532 nm laser illumination. Au/i-forms and Au/s-forms attained killing rates of 21% and 64%, respectively. The comparatively low inactivation of *E. coli* noted for Au/i-forms was attributed to their reduced proximity to pathogen surface. Nonetheless, the bactericidal activity of Au/s-forms was on par with many antibody-conjugated Au NPs exposed to coherent light with similar fluence. These studies validate M13 i-form and s-form polymorphs as photothermal bactericidal agents. Although the applications for visible laser illumination are limited to near-surface tissue treatment, the binding versatility of the viral template allows different Au NP shapes and sizes to be used to tune plasmon absorbance into the near-infrared enabling deep penetration of human tissue. In addition, the modular nature of the filamentous phage receptor-binding proteins potentially significantly extends the host range and utility of these remarkable dual-function nanoscaffolds for photothermal lysis of pathogens.

ASSOCIATED CONTENT

Supporting Information.

Transmission electron micrographs (TEM) of filaments and i-forms; Histogram of i-forms size distribution; TEM of representative Au/i-forms and Au/s-forms samples with bound Au NPs and Au nanorods; TEM of Au/i-forms, Au/s-forms and colloidal Au NPs after incubation with *E. coli*; Viability counts of control samples;

AUTHOR INFORMATION

Corresponding Author

*Email: haberer@ucr.edu

ORCID

Elaine D. Haberer: 0000-0002-3676-9079

Tam-Triet Ngo-Duc: 0000-0003-4545-4009

Zaira Alibay: 0000-0002-1335-9202

Joshua Plank: 0000-0002-8441-2920

Author Contributions

The manuscript was written through contributions of all authors. All authors have given approval to the final version of the manuscript. ‡These authors contributed equally.

Funding Sources

This material is based upon research supported by, or in part by, the U. S. Office of Naval Research under award number N00014-14-1-0799, the Regents' Faculty Fellowship, and the UCR Collaborative Seed Grant Program.

Notes

The authors declare no competing financial interest.

ACKNOWLEDGMENT

This material is based upon research supported by, or in part by, the U. S. Office of Naval Research under award number N00014-14-1-0799, the Regents' Faculty Fellowship, and the UCR Collaborative Seed Grant Program. This study made use of the TEM FEI Tecnai12 in the Central Facility for Advanced Microscopy and Microanalysis (CFAMM) and the Horiba LabRam/AIST-NT AFM in the Analytical Chemistry Instrumentation Facility (ACIF) at UC Riverside.

REFERENCES

(1) Neu, H. C. The Crisis in Antibiotic Resistance. *Science* **1992**, *257* (5073), 1064–1073.

(2) Fischbach, M. A.; Walsh, C. T. Antibiotics for Emerging Pathogens. *Science* **2009**, *325* (5944), 1089–1093.

(3) Levy, S. B.; Bonnie, M. Antibacterial Resistance Worldwide: Causes, Challenges and Responses. *Nat. Med.* **2004**, *10* (12S), S122–S129.

(4) Feng, Y.; Liu, L.; Zhang, J.; Aslan, H.; Dong, M. Photoactive Antimicrobial Nanomaterials. *J. Mater. Chem. B* **2017**, *5* (44), 8631–8652.

(5) Zharov, V. P.; Mercer, K. E.; Galitovskaya, E. N.; Smeltzer, M. S. Photothermal Nanotherapeutics and Nanodiagnostics for Selective Killing of Bacteria Targeted with Gold Nanoparticles. *Biophys. J.* **2006**, *90* (2), 619–627.

(6) Khlebtsov, B.; Zharov, V.; Melnikov, A.; Tuchin, V.; Khlebtsov, N. Optical Amplification of Photothermal Therapy with Gold Nanoparticles and Nanoclusters. *Nanotechnology* **2006**, *17* (20), 5167–5179.

(7) Hu, B.; Zhang, L. P.; Chen, X. W.; Wang, J. H. Gold Nanorod-Covered Kanamycin-Loaded Hollow SiO2 (HSKAu Rod) Nanocapsules for Drug Delivery and Photothermal Therapy on Bacteria. *Nanoscale* **2013**, *5* (1), 246–252.

(8) Liz-Marzán, L. M. Tailoring Surface Plasmons through the Morphology and Assembly of Metal Nanoparticles. *Langmuir* **2006**, *22* (1), 32–41.

(9) Boisselier, E.; Astruc, D. Gold Nanoparticles in Nanomedicine: Preparations, Imaging, Diagnostics, Therapies and Toxicity. *Chem. Soc. Rev.* **2009**, *38* (6), 1759–1782.

(10) Millenbaugh, N. J.; Baskin, J. B.; DeSilva, M. N.; Elliott, W. R.; Glickman, R. D. Photothermal Killing of Staphylococcus Aureus Using Antibody-Targeted Gold

Nanoparticles. *Int. J. Nanomedicine* **2015**, *10*, 1953–1960.

(11) Mocan, L.; Matea, C.; Tabaran, F. A.; Mosteanu, O.; Pop, T.; Puia, C.; Agoston-Coldea, L.; Gonciar, D.; Kalman, E.; Zaharie, G.; Iancu, C.; Mocan, T. Selective in Vitro Photothermal Nano-Therapy of MRSA Infections Mediated by IgG Conjugated Gold Nanoparticles. *Sci. Rep.* **2016**, *6*, 39466.

(12) Norman, R. S.; Stone, J. W.; Gole, A.; Murphy, C. J.; Sabo-Attwood, T. L. Targeted Photothermal Lysis of the Pathogenic Bacteria, Pseudomonas Aeruginosa, with Gold Nanorods. *Nano Lett.* **2008**, 8 (1) 302-306.

(13) Teng, C. P.; Zhou, T.; Ye, E.; Liu, S.; Koh, L. D.; Low, M.; Loh, X. J.; Win, K. Y.; Zhang, L.; Han, M.-Y. Effective Targeted Photothermal Ablation of Multidrug Resistant Bacteria and Their Biofilms with NIR-Absorbing Gold Nanocrosses. *Adv. Healthc. Mater.* **2016**, *5* (16), 2122–2130.

(14) Fan, Z.; Senapati, D.; Khan, S. A.; Singh, A. K.; Hamme, A.; Yust, B.; Sardar, D.; Ray, P. C. Popcorn-Shaped Magnetic Core-Plasmonic Shell Multifunctional Nanoparticles for the Targeted Magnetic Separation and Enrichment, Label-Free SERS Imaging, and Photothermal Destruction of Multidrug-Resistant Bacteria. *Chem. - A Eur. J.* **2013**, *19* (8), 2839–2847.

(15) Dai, X.; Fan, Z.; Lu, Y.; Ray, P. C. Multifunctional Nanoplatforms for Targeted Multidrug-Resistant-Bacteria Theranostic Applications. *ACS Appl. Mater. Interfaces* **2013**, *5* (21), 11348–11354.

(16) Gu, F. X.; Karnik, R.; Wang, A. Z.; Alexis, F.; Levy-Nissenbaum, E.; Hong, S.; Langer, R. S.; Farokhzad, O. C. Targeted Nanoparticles for Cancer Therapy. *Nano Today* **2007**, *2* (3), 14–21.

(17) Chames, P.; Van Regenmortel, M.; Weiss, E.; Baty, D. Therapeutic Antibodies: Successes, Limitations and Hopes for the Future. *Br. J. Pharmacol.* **2009**, *157* (2), 220–233.

(18) Carter, T.; Mulholland, P.; Chester, K. Antibody-Targeted Nanoparticles for Cancer Treatment. *Immunotherapy* **2016**, *8* (8), 941–958.

(19) Groff, K.; Brown, J.; Clippinger, A. J. Modern Affinity Reagents: Recombinant Antibodies and Aptamers. *Biotechnol. Adv.* **2015**, *33* (8), 1787–1798.

(20) Šmuc, T.; Ahn, I. Y.; Ulrich, H. Nucleic Acid Aptamers as High Affinity Ligands in Biotechnology and Biosensorics. *J. Pharm. Biomed. Anal.* **2013**, *81–82*, 210–217.

(21) Kim, B.; Kim, E.; Yoo, Y.-J.; Bae, H.-W.; Chung, I.-Y.; Cho, Y.-H. Phage-Derived Antibacterials: Harnessing the Simplicity, Plasticity, and Diversity of Phages. *Viruses* **2019**, *11* (3), 268.

(22) Santos, S. B.; Costa, A. R.; Carvalho, C.; Nóbrega, F. L.; Azeredo, J. Exploiting Bacteriophage Proteomes: The Hidden Biotechnological Potential. *Trends Biotechnol.* **2018**, *36* (9), 966–984.

(23) Lin, A.; Jimenez, J.; Derr, J.; Vera, P.; Manapat, M. L.; Esvelt, K. M.; Villanueva, L.; Liu, D. R.; Chen, I. A. Inhibition of Bacterial Conjugation by Phage M13 and Its Protein G3p: Quantitative Analysis and Model. *PLoS One* **2011**, *6* (5), 19991.

(24) Omidfar, K.; Daneshpour, M. Advances in Phage Display Technology for Drug Discovery. *Expert Opin. Drug Discov.* **2015**, *10* (6), 651–669.

(25) Brown, K. Peptidic Tumor Targeting Agents: The Road from Phage Display Peptide Selections to Clinical Applications. *Curr. Pharm. Des.* **2010**, *16* (9), 1040–1054.

(26) Barbas, C.F., Burton, D.R., Scott, J. K., Silverman, G. J. *Phage Display: A Laboratory*

Manual; CSHL Press, 2004.

(27) Bardhan, N. M.; Ghosh, D.; Belcher, A. M. M13 Virus Based Detection of Bacterial Infections in Living Hosts. *J. Biophotonics* **2014**, *7* (8), 617–623.

(28) Peng, H.; Chen, I. A. Rapid Colorimetric Detection of Bacterial Species through the Capture of Gold Nanoparticles by Chimeric Phages. *ACS Nano* **2019**, *13* (2), 1244–1252.

(29) Heilpern, A. J.; Waldor, M. K. PIIICTX, a Predicted CTXφ Minor Coat Protein, Can Expand the Host Range of Coliphage Fd to Include Vibrio Cholerae. *J. Bacteriol.* **2003**, *185* (3), 1037–1044.

(30) Marzari, R.; Sblattero, D.; Righi, M.; Bradbury, A. Extending Filamentous Phage Host Range by the Grafting of a Heterologous Receptor Binding Domain. *Gene* **1997**, *185* (1), 27–33.

(31) Benjamin, C. E.; Chen, Z.; Kang, P.; Wilson, B. A.; Li, N.; Nielsen, S. O.; Qin, Z.; Gassensmith, J. J. Site-Selective Nucleation and Size Control of Gold Nanoparticle Photothermal Antennae on the Pore Structures of a Virus. *J. Am. Chem. Soc.* **2018**.

(32) Manning, M.; Moore, M.; Spremulli, L.; Griffith, J. Coat Protein Conformation in M13 Filaments, I-Forms and Spheroids. *Biochem. Biophys. Res. Commun.* **1983**, *112* (2), 349–355.

(33) Manning, M.; Griffith, J. Association of M13 I-Forms and Spheroids with Lipid Vesicles. *Arch. Biochem. Biophys.* **1985**, *236* (1), 297–303.

(34) Huang, Y.; Chiang, C. Y.; Lee, S. K.; Gao, Y.; Hu, E. L.; De Yoreo, J.; Belcher, A. M. Programmable Assembly of Nanoarchitectures Using Genetically Engineered Viruses. *Nano Lett.* **2005**, *5* (7), 1429–1434.

(35) Ngo-Duc, T. T.; Plank, J. M.; Chen, G.; Harrison, R. E. S.; Morikis, D.; Liu, H.; Haberer,

E. D. M13 Bacteriophage Spheroids as Scaffolds for Directed Synthesis of Spiky Gold Nanostructures. *Nanoscale* **2018**, *10* (27), 13055–13063.

(36) Manning, M.; Chrysogelos, S.; Griffith, J. Mechanism of Coliphage M13 Contraction: Intermediate Structures Trapped at Low Temperatures. *J. Virol.* **1981**, *40* (3), 912–919.

(37) Lopez, J.; Webster, R. E. Minor Coat Protein Composition and Location of the A Protein in Bacteriophage F1 Spheroids and I-Forms. *J Virol* **1982**, *42* (3), 1099–1107.

(38) Marvin, D. A.; Symmons, M. F.; Straus, S. K. Structure and Assembly of Filamentous Bacteriophages. *Prog. Biophys. Mol. Biol.* **2014**, *114* (2), 80–122.

(39) Griffith, J.; Manning, M.; Dunn, K. Filamentous Bacteriophage Contract into Hollow Spherical Particles upon Exposure to a Chloroform-Water Interface. *Cell* **1981**, *23* (3), 747–753.

(40) Manning, M.; Chrysogelos, S.; Griffith, J. Mechanism of Coliphage M13 Contraction: Intermediate Structures Trapped at Low Temperatures. *J. Virol.* **1981**, *40* (3), 912–919.

(41) Olsen, E. V.; Sykora, J. C.; Sorokulova, I. B.; Chen, I.-H.; Neely, W. C.; Barbaree, J. M.; Petrenko, V. A.; Vodyanoy, V. J. Phage Fusion Proteins As Bioselective Receptors For Piezoelectric Sensors E.V. Olsen. *ECS Trans.* **2007**, *2* (19), 9–25.

(42) Jacobson, A. Role of F Pili in the Penetration of Bacteriophage Fl. *J. Virol.* **1972**, *10* (4), 835–843.

(43) Shipway, A. N.; Lahav, M.; Gabai, R.; Willner, I. Investigations into the Electrostatically Induced Aggregation of Au Nanoparticles. *Langmuir* **2000**, *16* (23), 8789–8795.

(44) Ghosh, S. K.; Pal, T. Interparticle Coupling Effect on the Surface Plasmon Resonance of Gold Nanoparticles: From Theory to Applications. *Chemical Reviews*. American Chemical Society 2007, pp 4797–4862.

(45) Mayya, K. S.; Patil, V.; Sastry, M. On the Stability of Carboxylic Acid Derivatized Gold Colloidal Particles: The Role of Colloidal Solution PH Studied by Optical Absorption Spectroscopy. *Langmuir* **1997**, *13* (15), 3944–3947.

(46) Schatz, G. C. Electrodynamics of Nonspherical Noble Metal Nanoparticles and Nanoparticle Aggregates. *J. Mol. Struct. THEOCHEM* **2001**, *573* (1–3), 73–80.

(47) Riley, R. S.; Day, E. S. Gold Nanoparticle-Mediated Photothermal Therapy: Applications and Opportunities for Multimodal Cancer Treatment. *Wiley Interdiscip. Rev. Nanomedicine Nanobiotechnology* **2017**, *9* (4), 1449.

(48) Uusitalo, S.; Kögler, M.; Välimaa, A. L.; Popov, A.; Ryabchikov, Y.; Kontturi, V.; Siitonen, S.; Petäjä, J.; Virtanen, T.; Laitinen, R.; Kinnunen, M.; Meglinski, I.; Kabashin, A.; Bunker, A.; Viitalab, T.; Hiltunen, J. Detection of: Listeria Innocua on Roll-to-Roll Produced SERS Substrates with Gold Nanoparticles. *RSC Adv.* **2016**, *6* (67), 62981–62989.

(49) Kirui, D. K.; Weber, G.; Talackine, J.; Millenbaugh, N. J. Targeted Laser Therapy Synergistically Enhances Efficacy of Antibiotics against Multi-Drug Resistant Staphylococcus Aureus and Pseudomonas Aeruginosa Biofilms. *Nanomedicine Nanotechnology, Biol. Med.* **2019**, *20*, 102018.

(50) Jacobson, A. Role of F Pili in the Penetration of Bacteriophage Fl. *J. Virol.* **1972**, *10* (4), 835–843.

(51) Sowa, B. A.; Moore, D.; Ippen Ihler, K. Physiology of F-Pilin Synthesis and Utilization. *J. Bacteriol.* **1983**.

(52) Novotny, C. P.; Fives Taylor, P. Retraction of F Pili. *J. Bacteriol.* **1974**.

(53) BRINTON, C. C.; GEMSKI, P.; CARNAHAN, J. A New Type of Bacterial Pilus

Genetically Controlled By the Fertility. *Proc. Natl. Acad. Sci. United States* **1964**, *52* (3), 776–783.

(54) Biebricher, C. K.; DUker, E.-M. F and Type 1 Piliation of Escherichia Coli. *Microbiology* **1984**, *130* (4), 951–957.

(55) Huang, X.; Jain, P. K.; El-Sayed, I. H.; El-Sayed, M. A. Plasmonic Photothermal Therapy (PPTT) Using Gold Nanoparticles. *Lasers Med. Sci.* **2008**, *23* (3), 217–228.

(56) Coronado, E. A.; Encina, E. R.; Stefani, F. D. Optical Properties of Metallic Nanoparticles: Manipulating Light, Heat and Forces at the Nanoscale. *Nanoscale* **2011**, *3* (10), 4042–4059.

(57) Bendix, P. M.; Reihani, S. N. S.; Oddershede, L. B. Direct Measurements of Heating by Electromagnetically Trapped Gold Nanoparticles on Supported Lipid Bilayers. *ACS Nano* **2010**, *4* (4), 2256–2262.

(58) Tzagoloff, H.; Pratt, D. The Initial Steps in Infection with Coliphage M13. *Virology* **1964**.

(59) Govorov, A. O.; Richardson, H. H. Generating Heat with Metal Nanoparticles. *Nano Today* **2007**, *2* (1), 30–38.

(60) Govorov, A. O.; Zhang, W.; Skeini, T.; Richardson, H.; Lee, J.; Kotov, N. A. Gold Nanoparticle Ensembles as Heaters and Actuators: Melting and Collective Plasmon Resonances. *Nanoscale Res. Lett.* **2006**, *1* (1), 84–90.

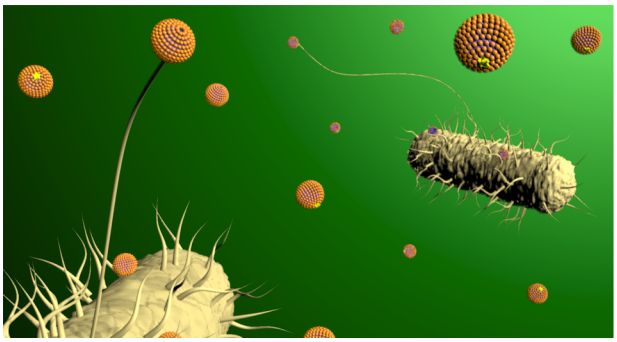

For Table of Contents Only